


Article

Generalized Control of the Power Flow in Local Area Energy Networks

Paolo Tenti ¹ and Tommaso Caldognetto ^{2,*} ¹ Department of Information Engineering, University of Padova, 35131 Padova, Italy; paolo.tenti@unipd.it² Department of Management and Engineering, University of Padova, 36100 Vicenza, Italy

* Correspondence: tommaso.caldognetto@unipd.it

Abstract: Local area energy networks (E-LANs) are cyber-physical systems whose physical layer is a meshed low-voltage microgrid fed by a multiplicity of sources, i.e., utilities, energy storage systems, and distributed power sources. The cyber layer includes distributed measurement, control, and communication units, located at end-user premises, as well as centralized supervision and dispatchment control. As compared with standard microgrid, the E-LAN encompasses the ability for end-users to actively contribute to the operation of the microgrid while acting as independent energy traders in the electrical market. Operational goals include active contribution of end-users to power sharing, loss reduction, voltage stability, demand response, fault identification and clearing, isolation of sub-grids for maintenance, islanding, and black start. Economic goals include the possibility, for each end-user, to decide in every moment, based on convenience, how his energy and power capacity is shared with other users, e.g., for demand response or to trade energy in the electric market. This paper introduces a comprehensive theoretical approach of E-LAN control to achieve all the above operational goals while providing a high level of dynamic protection against faults or other events affecting the system functionality, e.g., overloads or fast transients. It shows that meshed microgrids are the necessary infrastructure to implement the desired functionalities.

Keywords: control of distributed energy resources; power flow control; microgrids; distributed electronic power converters; demand response



Citation: Tenti, P.; Caldognetto, T. Generalized Control of the Power Flow in Local Area Energy Networks. *Energies* **2022**, *15*, 1416. <https://doi.org/10.3390/en15041416>

Academic Editor: Juri Belikov

Received: 30 December 2021

Accepted: 10 February 2022

Published: 15 February 2022

Publisher's Note: MDPI stays neutral with regard to jurisdictional claims in published maps and institutional affiliations.



Copyright: © 2022 by the authors. Licensee MDPI, Basel, Switzerland. This article is an open access article distributed under the terms and conditions of the Creative Commons Attribution (CC BY) license (<https://creativecommons.org/licenses/by/4.0/>).

1. Introduction

The future of electric systems is characterized by the increasing participation of end-users to fill the gap between energy demand and supply while ensuring the flexibility needed to face and to exploit the increasing complexity, decentralization, and interconnection of power systems. While in the first phase of the green energy transition the end-users acted as distributed investors and renewable energy suppliers, in future they will gain a role as market players, either individually or in aggregated form [1,2]. This was explicitly envisioned by the European Union within the 2019 directive “Clean Energy for All Europeans” that states “Consumers are the drivers of the energy transition” and “Consumers and communities will be empowered to actively participate in the electricity market” [3].

A first step in this direction is represented by virtual power plants (VPPs) [4] that are cloud-based distributed power plants that aggregate the capacities of heterogeneous distributed energy resources for the purposes of enhancing power generation, as well as trading or selling power on the electricity market.

With this approach, end-users virtually commit their energy resources to an aggregator that gathers consumers for the purpose of negotiating the rate for generation service from electric system operators. In this way, the participation of end-users to the electric market is indirect. Moreover, since there is no physical interaction among virtually connected users, their resources cannot be exploited to improve the performance and extend the functionality of electrical systems.

Today, the aggregation of users within virtual power plants (VPPs) is already a reality in several instances [5,6], and helps improving the flexibility of the electric system in the low-end section.

A completely different approach relies on local area energy networks (E-LANs) that aggregate the users within a microgrid and coordinate their operation to improve the electric performances, extend the grid functionalities, and allow participation of end-users to the electric market either individually or within energy communities [7].

In principle, each user may decide, time by time, which part of his capacity (stored energy, active and reactive power) can be shared with the rest of the E-LAN to improve local performance (e.g., voltage stabilization, loss reduction, power sharing, stress reduction) or to meet system-level requirements (e.g., demand response, power factor at the point of common coupling with utility, transition from on-grid to off-grid operation, fault clearing, etc.). The remaining capacity can be used for private needs, e.g., smoothing of domestic power absorption or trading energy in the market [2,8].

The E-LAN controller manages the available resources to pursue the needed functionalities, properly prioritized, with a best-fit approach. Obviously, the envisioned flexibility of operation calls for energy storage capacity, either distributed or clustered.

From the above considerations it follows that, unlike traditional microgrids, E-LANs represent a special type of cyber-physical systems where the physical layer (the microgrid) is thoroughly interconnected with the cyber layer [9]. Energy and data processing proceed indissolubly, and the implementation of the above functionalities require, on one side, fast and precise control of the power flow in each section of the microgrid and, on the other side, fast and precise implementation of the control algorithms, either distributed or centralized.

The fundamental asset of E-LANs is the capacity to implement the power steering, i.e., to exploit every available control agent to drive the power flow in every section of the microgrid. This requires meshed architectures and a suitable number of controlling entities distributed within the microgrid.

In the following, we will approach the problem at large, discussing the properties of meshed grids at first, then deriving the input–output equations valid for any type of grid structure and distribution of power sources, and finally proposing an optimum control approach that ensures all needed functionalities while allowing dynamic tuning of users' behavior and parameters.

2. Meshed Grids: Motivation and Basic Equations

2.1. Motivation

Traditionally, electric plants use radial structure, where any pair of nodes are linked by a single path. This results in simple design, because the current stress in each feeder can easily be predicted in every operating condition. Moreover, selective protection against faults is effectively achieved by operating the upstream protection devices (e.g., circuit breakers or fuses). Figure 1 shows the evolution of a distribution network, from the purely unidirectional radial structure (Figure 1a) fed via the connection to an upstream—typically medium voltage—distribution grid, to a situation where the radial grid is permeated by distributed generators (DGs) enabling bidirectional power flow (Figure 1b), to the most advanced solution that makes use of meshed grids (Figure 1c) to improve the flexibility of power flow control and the robustness of the electrical service. In practice, adopting a radial structure for the microgrid makes it impossible to drive the power through different paths, thus making the power steering unfeasible.

Meshed grids, instead, in presence of a suitable number of control agents (i.e., power electronics converters [10,11]), allow both power steering and autonomous participation of end-users to the electric market [12]. In this context, control agents correspond to energy sources equipped with grid-tied inverters able to control the active and reactive power exchange with the grid.

Synergistic operation of control agents enables the following functionalities:

- Control of the power flow throughout the microgrid (power steering).

- Consensus-based exploitation of any available energy sources (power sharing, smart energy storage).
- Mitigation of useless circulation of active and reactive currents.
- Stabilization of voltage profiles
- Compensation of load unbalance.
- Electronic fault clearing.
- Demand response.
- Off-grid operation.
- Autonomous energy trading by end-users who can decide, time by time, which portion of their resources is shared with the energy community.

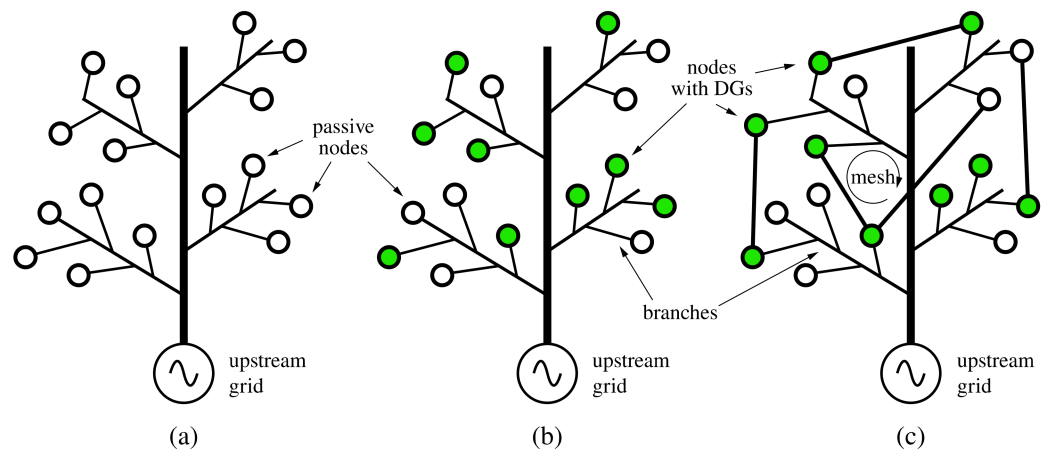


Figure 1. Different kinds of distribution networks. (a) Radial with passive nodes; (b) radial with distributed generators (DGs); (c) meshed with DGs.

Modern electricity scenarios foresee the possibility of trading the above operational functionalities as services for the upstream grid and therefore achieve economic benefits. In order to manage the system complexity and ensure a modular organization of E-LAN control, this typically involves the integration of economic and market layers in control hierarchy [2,13].

2.2. Basic Equations

The basic equations relating the voltages and currents in a microgrid are those determined by Kirchhoff's principles [14], which are reported below to define the nomenclature used herein.

Let \mathbf{A} be the incidence matrix describing the graph of the microgrid. \mathbf{A} is an integer matrix with K rows (K being the number of grid branches, i.e., lines connecting pairs of nodes) and N columns (N being the number of all grid nodes but node 0 associated to voltage reference V_0). The generic element a_{kn} of matrix \mathbf{A} is -1 if branch k begins in node n , $+1$ if branch k ends in node n , 0 otherwise. Connections to reference node 0 are neglected.

In the following, to determine voltage relations that do not depend on the selected reference V_0 , we will refer to node voltage deviations \mathbf{u} in place of node voltages \mathbf{v} (for generic node n , voltage deviation is: $\mathbf{u}_n = \mathbf{v}_n - V_0$).

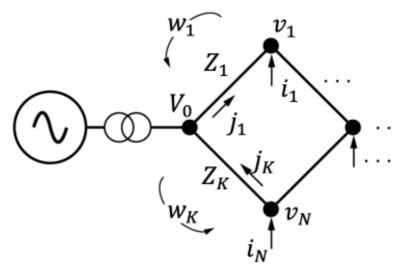
Based on matrix \mathbf{A} definition, the relation among node voltage deviations \mathbf{u} and branch voltages \mathbf{w} obeys the Kirchhoff's law for voltages (KLV) and is expressed by

$$\mathbf{w} = \mathbf{A} \mathbf{u}, \quad (1a)$$

Similarly, the relation among branch currents \mathbf{j} and node currents \mathbf{i} (i.e., the currents entering network nodes) obeys the Kirchhoff law for currents (KLC) and is expressed by:

$$\mathbf{i} = \mathbf{A}^T \mathbf{j}, \quad (1b)$$

where superscript T means matrix transpose. The meaning of the used nomenclature is sketched in Figure 2, which refers to the nodes and links of a single mesh.



Explanation of nomenclature:

$u_n = v_n - V_0$: voltage deviation at node n

i_n : current entering network at node n

w_n : voltage across branch n

j_n : current flowing in branch n

Z_n : impedance of branch n

Figure 2. Nomenclature for the nodes and branches of a single mesh.

The considerations reported hereafter hold both for DC and AC grids. In the latter case, we refer to sinusoidal operation where currents and voltages are represented by phasors in the complex domain. For the sake of simplicity, we will only treat the case of AC grids. In the case of DC grids, the complex variables and matrices will be substituted by real quantities.

In radial grids, matrix \mathbf{A} is invertible, thus the inverse of Equation (1) is easily obtained. Instead, in meshed grids the actual distribution of currents among the grid branches depends on their impedances; similarly, for the relation between branch voltages and node voltages. Letting \mathbf{Z} be the diagonal matrix of branch impedances, expressed as complex numbers, the relation among branch voltages \mathbf{w} and branch currents \mathbf{j} is

$$\mathbf{w} = \mathbf{Z} \mathbf{j} \Leftrightarrow \mathbf{j} = \mathbf{Z}^{-1} \mathbf{w}, \quad (2)$$

The relation among node currents \mathbf{i} and node voltage deviations \mathbf{u} , is:

$$\mathbf{i} = \mathbf{Y} \mathbf{u} \Leftrightarrow \mathbf{u} = \mathbf{Y}^{-1} \mathbf{i}, \quad (3a)$$

where \mathbf{Y} is the nodal admittance matrix, given by

$$\mathbf{Y} = \mathbf{A}^T \mathbf{Z}^{-1} \mathbf{A} \quad (3b)$$

Let us define the pseudo-inverse \mathbf{B} of matrix \mathbf{A} as

$$\mathbf{B} = \mathbf{Y}^{-1} \mathbf{A}^T \mathbf{Z}^{-1} \Rightarrow \mathbf{B} \mathbf{A} = \text{identity}, \quad (4)$$

We can now introduce the inverse of relations (1) as

$$\mathbf{u} = \mathbf{B} \mathbf{w}, \quad (5a)$$

$$\mathbf{j} = \mathbf{B}^T \mathbf{i}, \quad (5b)$$

The above set of complex equations allows a complete analysis of the microgrid operation for any given set of voltages and currents fed at the network nodes by the loads and sources connected therein.

3. Low-Voltage E-LAN: Structure and Input/Output Equations

The concept scheme of a low-voltage E-LAN is shown in Figure 3.

The E-LAN includes a LV distribution network with K branches, each one characterized by its length and impedance, and N nodes, where loads and sources are connected. The equations of the distribution network are those derived in the previous section.

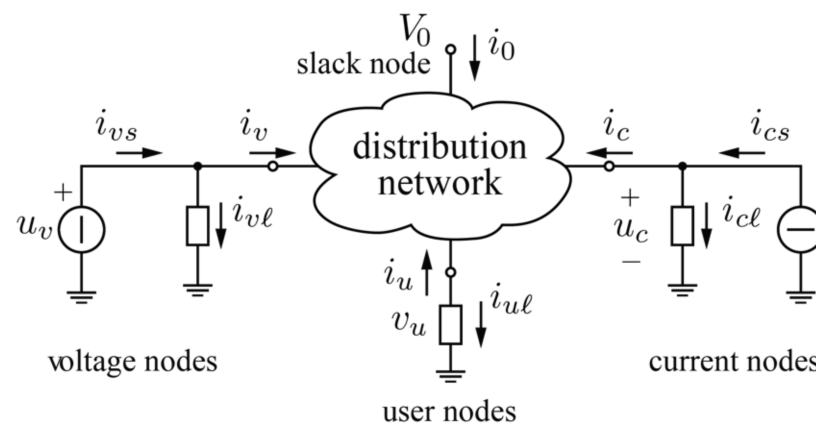


Figure 3. Concept scheme of E-LAN.

3.1. Node Classification

As shown in Figure 3, the nodes are classified in three groups:

- *Voltage nodes*, fed by voltage sources that can be uncontrollable (e.g., the secondary-side voltages of step-down transformers fed by the medium-voltage distribution system) or controllable (e.g., the voltages fed by voltage-driven converters interfacing energy sources with the distribution network). The voltage reference node normally corresponds to the point of common coupling (PCC) with the utility, where the network is fed by a nearly constant voltage V_0 which sets the amplitude and phase reference for any other grid voltages. This node is also called slack node, for its property to fill the gap between the power absorbed by the loads and that generated by the sources. In case of multiple PCCs, the most powerful node can be chosen as the voltage reference. Controllable voltage nodes may be used as voltage-forming units in case of off-grid operation and voltage-tracking units in case of on-grid operation. They are often interfacing the grid with the energy storage systems located in the proximity of the PCCs called utility interfaces (UIs).
- *Current nodes*, fed by current sources, namely, power sources tied to the distribution network by current-controlled converters. This definition generally applies to distributed renewable sources that, usually, operate as current sources that do not directly alter the voltage at their point of connection, to prevent instabilities in the distribution network.
- *Load nodes*, feeding purely passive loads.

Both voltage nodes and currents nodes can tie to passive loads in addition to the sources.

In the following, the analysis will be carried out with reference to a single-phase low-voltage microgrid, although it was developed for the general case of three-phase four-wire networks. In practice, as will be shown in the simulation section, actual loads and sources can be either single-phase or three-phase, their connection to the grid being phase-to-neutral, phase-to-phase, three-phase three-wires, or three-phase four-wires. The types of connection will be considered in the optimization procedure by introducing a suitable set of constraints on the amplitude and phase of the load and source currents.

3.2. Simplifying Assumptions

To simplify the analysis of low-voltage E-LANs, we observe that they extend over limited areas, with a number of users that cannot exceed few tens to comply with the power ratings of low-voltage distribution transformers. Considering the nearly resistive impedance of the LV distribution cables, we may assume that all voltages at grid nodes are nearly in phase with the reference voltage, their deviation being a few percent of the reference value.

Therefore, if we consider that all voltage phasors lie on the real axis, we may assume that the real components of the node currents correspond to active currents, while the imaginary components correspond to reactive currents.

Moreover, since node voltages are very close to the reference value, we may represent constant-power loads as constant-current loads.

The above assumptions introduce some inaccuracy, of course, but linearize the analysis of E-LAN operation, making it possible to find an explicit solution for the control problem. In fact, the nonlinear power-flow approach can be replaced by a linear current-flow approach that allows much easier analysis and reduced computational effort.

3.3. Node Selection

Let \mathbf{u} and \mathbf{i} be, respectively, the voltage deviations at the grid nodes and the corresponding currents entering the grid. We may express the electrical quantities at the voltage nodes as

$$\mathbf{u}_v = \mathbf{K}_v \mathbf{u}, \mathbf{i}_v = \mathbf{K}_v \mathbf{i}, \quad (6a)$$

where \mathbf{K}_v is the voltage node selector, i.e., an $N_v \times N$ integer matrix (with coefficients 0 or 1) that selects the N_v elements of vectors \mathbf{u} and \mathbf{i} corresponding to the node voltages. Similarly, for the N_c current nodes and the N_\downarrow load nodes, we can write

$$\mathbf{u}_c = \mathbf{K}_c \mathbf{u}, \mathbf{i}_c = \mathbf{K}_c \mathbf{i}, \quad (6b)$$

$$\mathbf{u}_\downarrow = \mathbf{K}_\downarrow \mathbf{u}, \mathbf{i}_\downarrow = \mathbf{K}_\downarrow \mathbf{i}, \quad (6c)$$

Given the voltages and the currents at the various types of nodes, the total node voltages and currents can be reconstructed by the reverse equations:

$$\mathbf{u} = \mathbf{K}_v^T \mathbf{u}_v + \mathbf{K}_c^T \mathbf{u}_c + \mathbf{K}_\downarrow^T \mathbf{u}_\downarrow, \mathbf{i} = \mathbf{K}_v^T \mathbf{i}_v + \mathbf{K}_c^T \mathbf{i}_c + \mathbf{K}_\downarrow^T \mathbf{i}_\downarrow, \quad (7)$$

The current terms in (6) are conventionally entering the grid. In practice, voltage and current sources can also feed loads connected to the same nodes; thus, the total currents fed by the sources are

$$\mathbf{i}_{vs} = \mathbf{i}_v + \mathbf{i}_{v\downarrow}, \mathbf{i}_{cs} = \mathbf{i}_c + \mathbf{i}_{c\downarrow}, \quad (8)$$

3.4. Input–Output Equations

From the above considerations, it turns out that the input variables, determining the operation of the distribution network, are voltages \mathbf{u}_v impressed at voltage nodes, currents \mathbf{i}_c impressed at current nodes, and load currents \mathbf{i}_\downarrow . The output variables are currents \mathbf{i}_v entering the grid at voltage nodes, voltages \mathbf{u}_c at current nodes, and voltages \mathbf{u}_\downarrow at load nodes. We define, for convenience, user currents \mathbf{i}_s and user voltages \mathbf{u}_s as

$$\mathbf{u}_s = \begin{bmatrix} \mathbf{u}_c \\ \mathbf{u}_\downarrow \end{bmatrix}, \mathbf{i}_s = \begin{bmatrix} \mathbf{i}_c \\ -\mathbf{i}_\downarrow \end{bmatrix}, \quad (9a)$$

Letting \mathbf{K}_s be the corresponding node selector, the input–output equations can therefore be expressed as

$$\begin{bmatrix} \mathbf{i}_v \\ \mathbf{i}_s \end{bmatrix} = \mathbf{H} \begin{bmatrix} \mathbf{u}_v \\ \mathbf{i}_s \end{bmatrix} = \begin{bmatrix} \mathbf{H}_{vv} & \mathbf{H}_{vs} \\ \mathbf{H}_{sv} & \mathbf{H}_{ss} \end{bmatrix} \begin{bmatrix} \mathbf{u}_v \\ \mathbf{i}_s \end{bmatrix}, \quad (9b)$$

where hybrid matrix \mathbf{H} is the input–output transfer matrix. It can be evaluated starting from the partitioned form of Equation (3a):

$$\begin{bmatrix} \mathbf{i}_v \\ \mathbf{i}_s \end{bmatrix} = \begin{bmatrix} \mathbf{Y}_{vv} & \mathbf{Y}_{vs} \\ \mathbf{Y}_{sv} & \mathbf{Y}_{ss} \end{bmatrix} \begin{bmatrix} \mathbf{u}_v \\ \mathbf{i}_s \end{bmatrix}, \left\{ \begin{array}{l} \mathbf{Y}_{vv} = \mathbf{K}_v \mathbf{Y} \mathbf{K}_v^T \\ \mathbf{Y}_{sv} = \mathbf{K}_s \mathbf{Y} \mathbf{K}_v^T \\ \mathbf{Y}_{vs} = \mathbf{K}_v \mathbf{Y} \mathbf{K}_s^T \\ \mathbf{Y}_{ss} = \mathbf{K}_s \mathbf{Y} \mathbf{K}_s^T \end{array} \right\}, \quad (9c)$$

In (9c) it is interesting to note that if one or more nodes change their operating mode, matrix \mathbf{Y} remains the same, while selection matrices \mathbf{K} change.

Now, combining (9b) and (9c), we easily derive the expression of matrix \mathbf{H} as

$$\mathbf{H} = \begin{bmatrix} \mathbf{H}_{vv} & \mathbf{H}_{vs} \\ \mathbf{H}_{sv} & \mathbf{H}_{ss} \end{bmatrix}, \left\{ \begin{array}{ll} \mathbf{H}_{vv} = \mathbf{Y}_{vv} - \mathbf{Y}_{vs} \mathbf{Y}_{ss}^{-1} \mathbf{Y}_{sv} & \mathbf{H}_{vs} = \mathbf{Y}_{vs} \mathbf{Y}_{ss}^{-1} \\ \mathbf{H}_{sv} = -\mathbf{Y}_{ss}^{-1} \mathbf{Y}_{sv} & \mathbf{H}_{ss} = \mathbf{Y}_{ss}^{-1} \end{array} \right\}, \quad (9d)$$

Observe that the computation of all submatrices of \mathbf{H} requires only one matrix inversion (\mathbf{Y}_{ss}^{-1}).

4. Control Variables

As mentioned before, the input variables determining network operation are voltages \mathbf{u}_v impressed at voltage nodes, and currents \mathbf{i}_s impressed at user nodes. Generally, these variables are not fully controllable. Thus, we can split the input variables in noncontrollable terms (superscript \circ) and controllable terms (superscript \sim):

$$\mathbf{u}_v = \mathbf{u}_v^\circ + \tilde{\mathbf{u}}_v, \quad (10a)$$

$$\mathbf{i}_s = \mathbf{i}_s^\circ + \tilde{\mathbf{i}}_s \quad (10b)$$

In practice, controllable terms may occur only for a limited set of input variables. Let \mathbf{K}_d be the selector of those voltages, among $\tilde{\mathbf{u}}_v$, whose phasor can be controlled on the real (direct) axis, and \mathbf{K}_q the selector of those voltages that can be controlled on the imaginary (quadrature) axis. Let \mathbf{u}_d be the controllable voltage terms along the direct axis, and \mathbf{u}_q the controllable voltage terms along the quadrature axis; similarly to (7), we may express voltages $\tilde{\mathbf{u}}_v$ as

$$\tilde{\mathbf{u}}_v = \mathbf{K}_d^T \mathbf{u}_d + \mathbf{K}_q^T \mathbf{u}_q \Rightarrow \mathbf{u}_v = \mathbf{u}_v^\circ + \mathbf{K}_d^T \mathbf{u}_d + \mathbf{K}_q^T \mathbf{u}_q, \quad (11a)$$

Similarly, we define \mathbf{K}_a as the selector, among $\tilde{\mathbf{i}}_s$, of current terms \mathbf{i}_a that can be controlled on the real axis (active currents, corresponding to the active power entering the grid at the corresponding nodes), and \mathbf{K}_r as the selector of terms \mathbf{i}_r that can be controlled on the imaginary axis (reactive currents, corresponding to the reactive power). We may therefore express currents $\tilde{\mathbf{i}}_s$ as

$$\tilde{\mathbf{i}}_s = \mathbf{K}_a^T \mathbf{i}_a + \mathbf{K}_r^T \mathbf{i}_r \Rightarrow \mathbf{i}_s = \mathbf{i}_s^\circ + \mathbf{K}_a^T \mathbf{i}_a + \mathbf{K}_r^T \mathbf{i}_r, \quad (11b)$$

Accordingly, the input variables for E-LAN control become real quantities $\mathbf{u}_d, \mathbf{u}_q, \mathbf{i}_a, \mathbf{i}_r$. Let \mathbf{x} be the real vector of control inputs:

$$\mathbf{x} = \begin{bmatrix} \mathbf{u}_d \\ \mathbf{u}_q \\ \mathbf{i}_a \\ \mathbf{i}_r \end{bmatrix}, \quad (11c)$$

By means of Equations (9) and (11) we can express all node voltages and currents in the form

$$\mathbf{u} = \mathbf{u}^0 + \mathbf{F}_u \mathbf{x}, \mathbf{i} = \mathbf{i}^0 + \mathbf{F}_i \mathbf{x}, \quad (12a)$$

While \mathbf{x} is a real vector, the other variables represent phasors in the complex plane. Constant matrices \mathbf{F} are complex and depend on grid structure and node types. Quantities with superscript $^\circ$ refer to the situation when all control inputs vanish (zero state).

Similarly, considering Equations (1a) and (5b), we can express branch voltages and currents as

$$\mathbf{w} = \mathbf{w}^0 + \mathbf{F}_w \mathbf{x}, \mathbf{j} = \mathbf{j}^0 + \mathbf{F}_j \mathbf{x}, \quad (12b)$$

The above expressions show that all relations between input and output variables are linear equations in the complex domain.

5. Optimum Control

Taking advantage of the linearity of control equations, we may approach the E-LAN control problem as a constrained optimum problem in L^2 space. For this purpose, we define a cost function that represents the grid performance from various perspectives. Then, we introduce a set of constraints that circumscribe the desired operating conditions.

5.1. Cost Function

The performances that we wish to optimize relate to voltage stability, energy efficiency, thermal stress of feeders, power stress of sources, and current stress of electronic power converters.

We therefore optimize a cost function φ including three weighted additive terms:

$$\varphi = \varphi_{loss} + \varphi_{stress} + \varphi_{dev}, \quad (13a)$$

- Term φ_{loss} accounts for total power loss, including transformer loss, distribution loss in feeders, and conversion loss in power converters.
- Term φ_{stress} accounts for current stress in feeders, active power stress in sources, and apparent power stress in grid-tied converters.
- Term φ_{dev} accounts for total rms voltage deviation at grid nodes.

All terms of the cost function can be expressed as quadratic functions of control inputs. Overall, the cost function can be expressed in the quadratic form

$$\varphi = a_{\varphi} + \mathbf{x}^T \mathbf{b}_{\varphi} + \mathbf{x}^T \mathbf{C}_{\varphi} \mathbf{x}, \quad (13b)$$

where coefficient a_{φ} , vector \mathbf{b}_{φ} , and matrix \mathbf{C}_{φ} are constant real quantities, depending on network parameters and zero state variables. In particular, \mathbf{C}_{φ} is a positive definite matrix.

5.2. Constraints

The E-LAN operation is normally analyzed under different conditions (operation modes) that depend on the daily variations of source and load power, on the state of charge of energy storage systems, and on specific requirements on the power flow, either stationary (e.g., relating to power balance, reactive power compensation, demand response) or dynamic (e.g., transition to and from islanding, black start, electronic fault clearing). In both single-phase (or DC) and three-phase applications, pursuing the desired operation modes implies constraints of the power flowing at specific network gates. Thanks to linearity of control equations, such power constraints can be expressed as a system of linear equations:

$$\boldsymbol{\psi} = \mathbf{b}_{\psi} + \mathbf{C}_{\psi} \mathbf{x}, \quad (14)$$

where vector \mathbf{b}_{ψ} and matrix \mathbf{C}_{ψ} are real, because the constraints on real and imaginary axes are considered separately.

As mentioned before, the constraints set by the types of connection of single-phase and three-phase loads and sources are also considered in (14) to allow an accurate representation of the actual grid operation.

5.3. Solution

The constrained optimum control problem can be solved in explicit form by the Lagrange multipliers method. Let $\boldsymbol{\lambda}$ be the vector of Lagrange multipliers, the solving system is

$$\begin{cases} \frac{\partial \varphi}{\partial \mathbf{x}} + \frac{\partial \boldsymbol{\psi}}{\partial \mathbf{x}} \boldsymbol{\lambda} = 0 \\ \boldsymbol{\psi} = 0 \end{cases}, \quad (15a)$$

Solving the system gives the optimum control variables as

$$\mathbf{x} = -\frac{1}{2}\mathbf{C}_\varphi^{-1}\left(\mathbf{C}_\psi^T\mathbf{C}_\lambda^{-1}\mathbf{b}_\lambda + \mathbf{b}_\varphi\right), \text{ with : } \begin{cases} \mathbf{C}_\lambda = \mathbf{C}_\psi\mathbf{C}_\varphi^{-1}\mathbf{C}_\psi^T \\ \mathbf{b}_\lambda = 2\mathbf{b}_\psi - \mathbf{C}_\psi\mathbf{C}_\varphi^{-1}\mathbf{b}_\varphi, \end{cases} \quad (15b)$$

Note that the solution only requires the inversion of two reduced-order matrices, namely \mathbf{C}_φ and \mathbf{C}_λ , to obtain the result in a single computation step.

Overall, the proposed approach is computationally efficient and can be adapted to any networks, irrespective of their structure and complexity. Further, it can be used to analyze the E-LAN operation in any operating conditions and with flexible definition of the performance function to be optimized.

6. Problem of Silent Nodes

The correct application of the above optimum control approach would require complete monitoring of the currents and voltages at any grid nodes. In actuality, this may be impossible or impractical, since at residential premises only rms voltage and active power are metered; junction nodes are not monitored at all; voltage phase is rarely measured, etc. In this section, we introduce an estimation methodology of network voltages and currents that allows implementation of the optimum solution even if monitoring applies to a limited set of nodes or electric quantities.

For the sake of simplicity, although not strictly necessary, we keep the assumption that all node voltages are real quantities, in phase with voltage reference V_0 . Let \mathbf{v}^m be the vector of measured node voltages, and \mathbf{v}^s be the vector of voltages at silent nodes, where measurement is not available. Similarly, define \mathbf{i}_a^m and \mathbf{i}_r^m as the vectors of measured active (real) and reactive (imaginary) currents entering grid nodes, and \mathbf{i}_a^s and \mathbf{i}_r^s the corresponding quantities at silent nodes. The problem is to estimate the unknown quantities at silent nodes given the quantities measured at monitored nodes. Let $\mathbf{\Gamma} = \mathbf{Y}^{-1}$ be the nodal impedance matrix of the network. Recalling that voltages \mathbf{v} and currents \mathbf{i}_a and \mathbf{i}_r are real quantities, letting ι be the imaginary unit and \mathcal{R} the real operator, we can write:

$$\mathbf{v} = \mathbf{\Gamma} \mathbf{i} \Rightarrow \begin{bmatrix} \mathbf{v}_m \\ \mathbf{v}_s \end{bmatrix} = \mathcal{R}\left(\begin{bmatrix} \mathbf{\Gamma}_m \\ \mathbf{\Gamma}_s \end{bmatrix} \begin{bmatrix} \mathbf{i} \end{bmatrix}\right) = \mathcal{R}\left(\begin{bmatrix} \mathbf{\Gamma}_m \\ \mathbf{\Gamma}_s \end{bmatrix} \left(\begin{bmatrix} \mathbf{i}_a^m \\ \mathbf{i}_a^s \end{bmatrix} + \iota \begin{bmatrix} \mathbf{i}_r^m \\ \mathbf{i}_r^s \end{bmatrix}\right)\right), \quad (16a)$$

Considering only the equations related to measured voltages \mathbf{v}_m , from (16a), we obtain

$$\mathbf{v}_m = \mathcal{R}\left(\begin{bmatrix} \mathbf{\Gamma}_{ma}^m & \mathbf{\Gamma}_{ms}^m \end{bmatrix} \begin{bmatrix} \mathbf{i}_a^m \\ \mathbf{i}_a^s \end{bmatrix} + \iota \begin{bmatrix} \mathbf{\Gamma}_{mr}^m & \mathbf{\Gamma}_{ms}^m \end{bmatrix} \begin{bmatrix} \mathbf{i}_r^m \\ \mathbf{i}_r^s \end{bmatrix}\right), \quad (16b)$$

where $\mathbf{\Gamma}_{ma}^m$ and $\mathbf{\Gamma}_{ms}^m$ are the submatrices of $\mathbf{\Gamma}_m$ that correspond to measured and nonmeasured active currents, and similarly $\mathbf{\Gamma}_{mr}^m$ and $\mathbf{\Gamma}_{ms}^m$ correspond to measured and nonmeasured reactive currents. Given the above submatrices, we can develop Equation (16b) to extract its real part, and then express the unknown quantities \mathbf{i}_a^s and \mathbf{i}_r^s as a function of measured quantities \mathbf{v}_m , \mathbf{i}_a^m , \mathbf{i}_r^m in the following form:

$$\mathbf{D} \begin{bmatrix} \mathbf{i}_a^s \\ \mathbf{i}_r^s \end{bmatrix} + \mathbf{e} = 0, \quad \begin{cases} \mathbf{D} = \mathbf{D}(\mathbf{\Gamma}_m) \\ \mathbf{e} = \mathbf{e}(\mathbf{\Gamma}_m, \mathbf{v}_m, \mathbf{i}_a^m, \mathbf{i}_r^m) \end{cases}, \quad (16c)$$

Matrix \mathbf{D} depends only on network parameters, while vector \mathbf{e} depends on measured quantities, too. Equation (16c) cannot be solved by inversion of matrix \mathbf{D} that, generally, has not full rank. We can therefore find a solution with Moore–Penrose pseudo-inverse approach, which finds the unknown currents which meet the network equations and minimize their total rms value. Given the estimates of currents \mathbf{i}_a^s and \mathbf{i}_r^s , unknown voltages \mathbf{v}_s can then be determined from the lower part of Equation (16a).

Obviously, the estimation is affected by an inaccuracy that is as higher as smaller is the number of monitored nodes. This approach, however, allows application of optimum

control in any situations. Several tests demonstrated that the errors on the control variables are quite limited in all practical cases where at load nodes only the active power is measured, while at source nodes both active and reactive power are measured together with the line voltage.

A different approach must be adopted for the estimation of load currents, which are input quantities for the optimum control. In this case, each load current is independent, and the evaluation is carried out by assuming that the unknown loads share the total power in the same proportion observed for the average of measured loads.

7. Application Example and Performance Assessment

A comprehensive simulation code (SUSI³, Smart Users & Sources Integration, Interconnection and Interplay) was developed to allow the analysis of the above control approach in networks of high complexity while offering a full set of options regarding the following:

- Network architecture and ratings (e.g., topology, distribution line impedances, current ratings of feeders, grid voltage and frequency, tolerance on impedance values).
- Types, connection, power and energy ratings, control ability, and operating constraints for any given categories of loads and sources.
- Daily profiles of source power generation and load absorption.
- Dynamic pricing of energy.
- Definition of case studies, in terms of operating conditions, control variables, node and branch constraints for power steering (e.g., active and reactive power flow at given network sections, phase power balance, power factor, saturation and tripping in case of overstress, etc.).
- Adjustment of cost function coefficients.

The simulation code provides a complete description of the grid operation in any selected operating conditions and timeframes (node quantities, branch quantities, aggregated power production and consumption for groups and categories of users and pricing, cumulative performance indexes such as power factor, unbalance factor, etc.).

Since the computation kernel is compact and efficient, the code can be implemented with fast simulation times even on standard desktop computers. For example, execution times considering networks with a hundred nodes is in the order of seconds if executed on a desktop PC with CPU Intel i5. This is compatible with typical power systems dynamics [15] and energy pricing variations [13].

7.1. The Considered Benchmark Network

As an example of application, the European low-voltage benchmark network proposed by CIGRE [16], shown in Figure 4, was considered. The network includes three sub-networks: residential, commercial, and industrial. The characteristics and parameters of loads, sources, and distribution feeders of the network are detailed in [16], and were considered for the simulation. Details on the considered network are reported in Appendix A, where, Table A1 specifies the type of feeders, Table A2 shows the connections among grid nodes, the characteristics of the loads tied to the grid, and the parameters of MV/LV transformers feeding the three sub-networks, and Table A3 specifies the characteristics of distributed energy sources.

As compared to the CIGRE benchmark network, wind turbines (WT), photovoltaic systems (PV), and distributed energy storage units (DES) similar to those proposed for the residential sub-network were added in the commercial and industrial sections, too. All distributed power sources, either RES (renewable energy sources) or DES, tie in to the grid by electronic power converters and perform as controllable current sources.

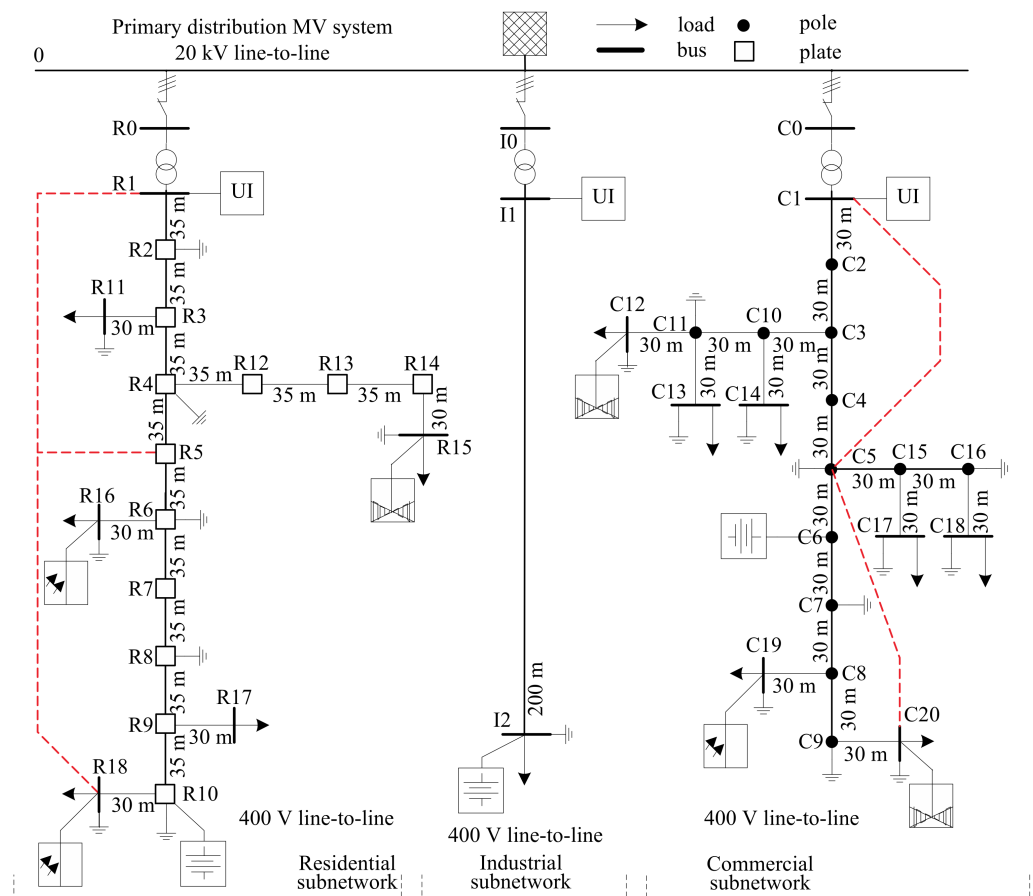


Figure 4. CIGRE European low-voltage network considered as application example.

To complement the network, we included the connecting lines shown in red color, that transform the original radial topology of each sub-network into a meshed one. In practice, this corresponds to duplicate the main power line in the cable duct.

Finally, utility interfaces (UIs) were added in each sub-network close to the PCC; these units, equipped with energy storage and three-phase PWM converters, perform as controllable voltage sources and act as voltage trackers during on-grid operation, and as voltage formers during off-grid operation [17–19]. Further to their voltage support action, these units allow reactive power and unbalance compensation in the proximity of each PCC, resulting in unity power factor at the utility terminals [20]. This action is possible thanks to the ability of three-phase grid-tied converters to exchange active power among the phases, and to generate compensating reactive power, without requiring net energy from the storage unit, the only limitation being due to the VA rating of the converter.

Utility interfaces and distributed energy storage units, as a whole, constitute the energy storage system (ESS).

We generally assume that load nodes only measure rms voltage and active power; RES and DES measure also reactive power for control purpose; finally, UIs measure voltage amplitude and phase, as needed to implement voltage tracking.

7.2. Radial versus Meshed Structure

A first set of simulation results are shown in Figure 5, where the network performances for radial and meshed topologies are compared. For this purpose, two quality indexes are considered. The first quality index is *total efficiency*, meant as the ratio between the total active power absorbed by loads and that generated by sources; all types of power loss (i.e., distribution, conversion, and generation loss) are considered in the computation. The second index is the *total voltage deviation*, meant as the cumulative rms value of the

differences between node voltages and the reference voltage. The upper part of the figure shows the daily profiles of the total active and reactive power absorbed by loads and the active power generated by renewable sources, computed according to typical CIGRE generation and consumption profiles. In this case, the ESS does not contribute to power generation, since DES and UIs are off. Moreover, RES converters do not generate reactive power. The lower part of the figure compares the performance of the radial and meshed configurations. As expected, for the given behavior of loads and sources, the meshed configuration provides better efficiency and lower voltage deviation, thanks to the multiple paths offered to the power to flow.

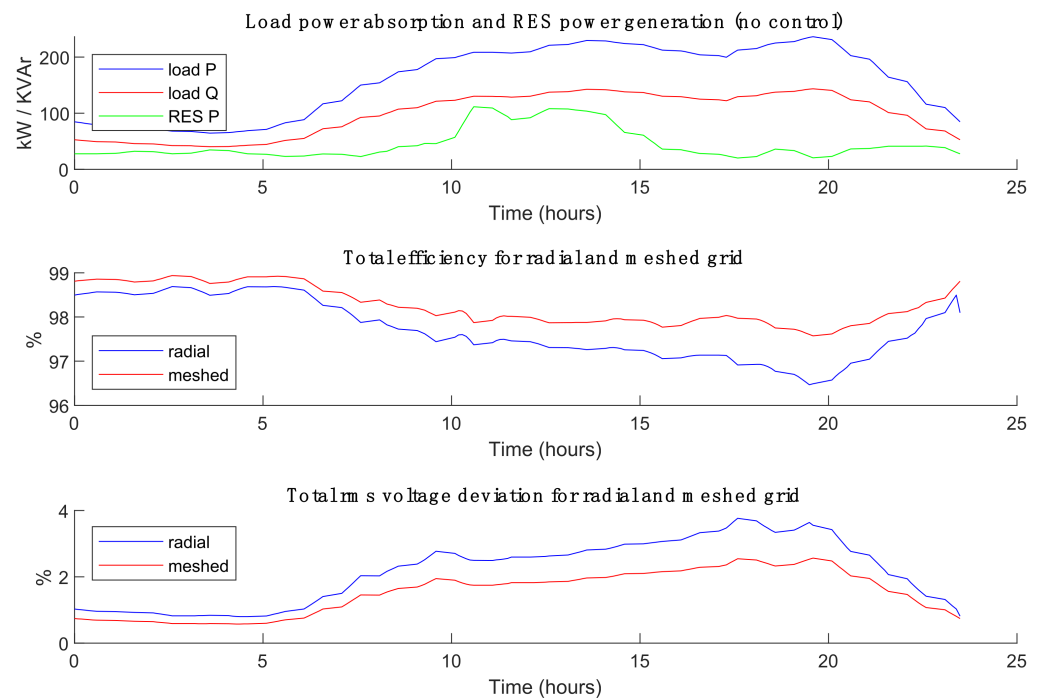


Figure 5. Comparison of quality indexes for radial and meshed network.

In the following, we will refer to the meshed topology, which—in addition to better performance indexes—allows full exploitation of the optimum control potentiality described above.

7.3. Impact of Reactive Power Control

Figure 6 aims at showing the effects of reactive power control, according to different techniques, which are referred to as Case 1–3 and discussed in the following. The above performance factors are considered again as indicators of the quality of performance.

- Case 1 refers to local reactive power compensation, when the converters interfacing the RES with the grid generate reactive power to compensate local loads. Obviously, the actual compensation capacity is limited by the VA rating of the converters. In this case, the control is merely local, and the central optimum control is not involved. The upper figure shows the reactive power sharing between utility and RES. The utility supplies the remaining reactive power, not locally provided by RES converters.
- In Case 2, the local reactive power compensation is complemented with the compensating action performed by ESS converters driven by the central optimum controller. The reactive power fed by the utility drops, evidently, the major burden of compensation being taken by the ESS. Note that the total reactive power fed by utility, DER, and ESS exceeds that required by the loads, and this is due to the optimum control that, in order to minimize the voltage deviation, creates a local injection of reactive power

at network nodes. As a result, while total efficiency remains almost the same as in Case 1, the voltage deviation reduces significantly.

- Finally, in Case 3, all controllable converters (RES and ESS) are driven by the central optimum controller. The reactive power sharing among utility, RES, and ESS changes considerably from the previous cases, since the reactive power required for RES vanishes, and the compensation task is substantially committed to ESS, with a minor contribution from the utility. The result is a significant improvement of total efficiency, while voltage deviation is similar to Case 2.

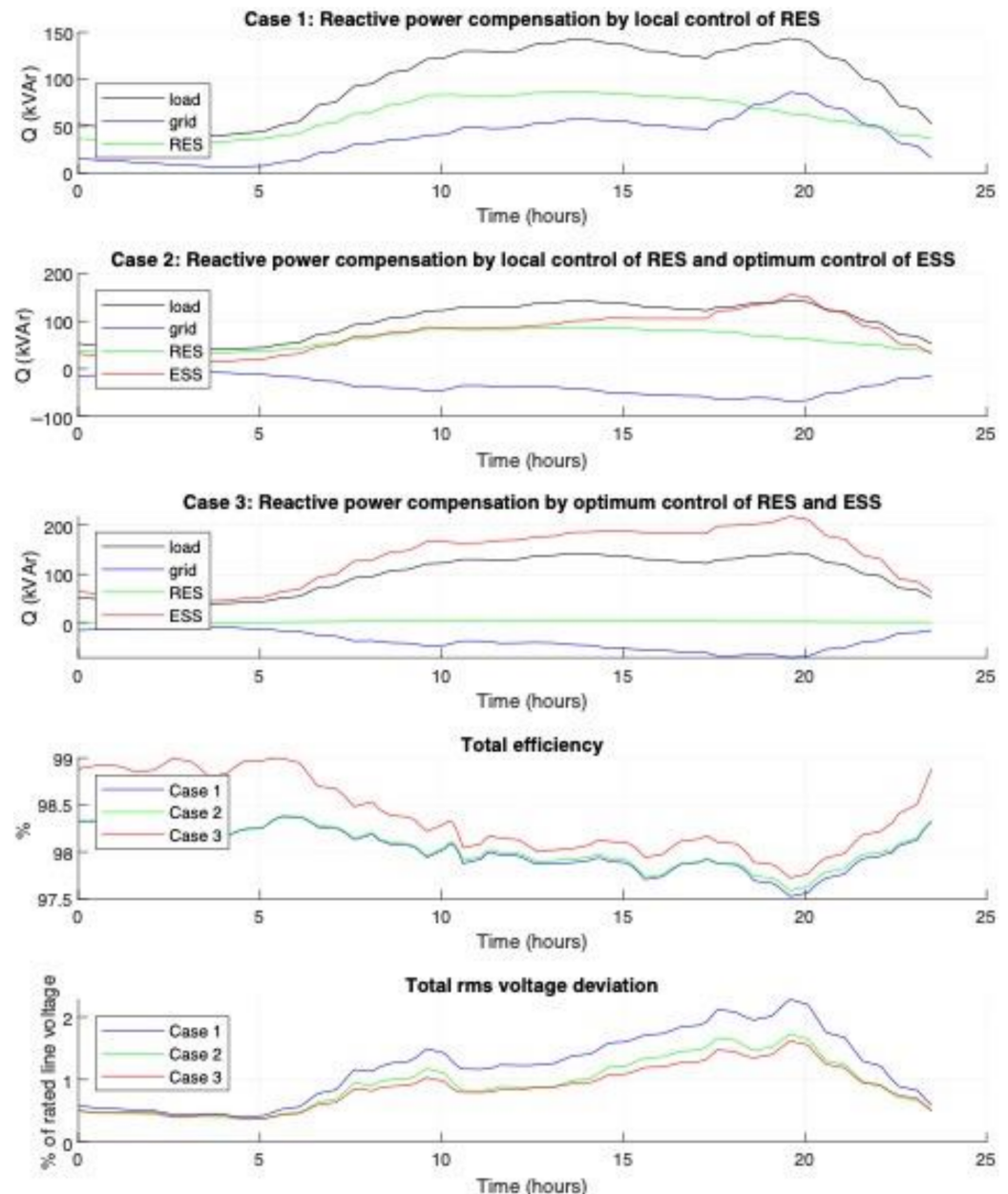


Figure 6. Results obtained considering different reactive power control methods.

Overall, this figure demonstrates that a suitable control of reactive power can significantly improve the network operation in terms of stability of the voltage profiles and reduction of power losses in the entire network.

7.4. Hybrid Control Operation

Figure 7 shows the daily network operation with hybrid control, i.e., local control of reactive power of RES units, whose active power is determined by renewable energy generation, and optimum control of all units equipped with energy storage (UIs and DES). Under regular operation, each ESS unit targets the nominal state of charge (SoC), while during transients they feed or store energy to suit network needs. At all times, the control ensures unity power factor at PCC, that is, balanced absorption of active power and no reactive power in all phases, and optimization of the global performance according to the selected cost function. During the daytime, load and source power profiles keep the same behavior shown in Figure 5. The regular operation is suspended three times, to suit the utility request:

- From 5 a.m. to 7 a.m., the network turns to islanded (i.e., off-grid) operation; correspondingly, the energy balance is ensured by the ESS, whose cumulative state of charge drops from 95% to 53% of the reference value for UIs, and from 95% to 72% for DES. Afterwards, the network returns to regular (i.e., on-grid) operation, and each ESS unit recharges at nominal SoC. This implies an extra power absorption from the utility for about 2.5 h, along which the recharge power of ESS is limited to 50% of rated power to preserve the lifetime of the batteries.
- From 10 a.m. to 11 a.m. and from 5 a.m. to 6 p.m., the power absorption of the network is reduced to 50% to halve the power fed by the utility. In this case, the utility and the ESS share the power demand of the network, and the cumulative SoC of batteries drops—to 70% in the first timeslot, and to 60% the second—and is recovered in the following recharge phases.

The lower part of the figure shows the behavior of the quality factors. The total efficiency keeps higher than 97.5% in all conditions, with an average value of 98%. The total rms voltage deviation keeps less than 2.5%, with an average value of 1.15%.

Overall, the figure shows the extreme flexibility of operation of the proposed control method, which allows effective exploitation of all the available resources while ensuring optimum performances from various perspectives: energy efficiency, voltage stability, thermal stresses in feeders, power stress of sources, and current stress of grid-tied converters.

Note, finally, that in the above examples, the utility requirements are met by exploiting only DES and UIs, the other sources being unaffected. In actuality, end users can individually decide on their participation to power control, as will be shown in the following.

7.5. Specific Features of the Proposed Control

The flexibility demonstrated by the previous examples derives from the methodological approach that pursues the optimization of a set of performance indexes while obeying a certain number of constraints. A proper selection of these constraints allows adaptation of E-LAN behavior to suit conditions that may considerably widen the usual range of operation of microgrids. Let us emphasize these aspects with reference to the previous examples.

- Active contribution of end-users to power-sharing.* Figure 6 shows the benefit of exploiting reactive power control by grid-tied inverters interfacing the distributed energy sources. In spite of the considerable improvement in terms of voltage stability, this ability is often disregarded, since inverters normally operate at unity power factor. In actuality, this feature can be implemented at local control level, that is, with limited modification of the inverters control algorithm. The contribution of end-users to active power balance could also be determinant; however, it is disregarded in Figure 7, where the total power demand halves (in intervals 11–12 a.m. and 5–6 p.m.) thanks only to the energy support provided by the common energy storage system (UIs and DES). In general, we may assume that the energy storage units installed at end-user premises are used to alleviate the energy bill of each individual prosumer. With the proposed approach, in fact, each end-user may decide how much of its power capacity is shared

with the rest of the microgrid to meet the objectives of centralized control and how much is kept available for local goals. Let us assume that every user node of the network of Figure 5 is equipped with an energy storage unit rated to meet the local power need for about two hours. This capacity is exploited to reduce the energy bill, by locally feeding the loads in those time intervals when the cost of energy is set high, specifically, +50% in the intervals 10–12 a.m. and 3–4 p.m.

Figure 8 shows the total load power absorption of end-users, together with the power locally fed by their energy storage units. The total power fed by the grid vanishes in the above intervals when the loads are fed at the expense of the locally stored energy. The state of charge of local energy storage is then recovered during the night, when the cost of energy drops by 50%. Overall, this causes, for end users, a net saving of energy bill of about 15%.

- (b) *Demand response.* This highly rewarding feature is inherently allowed by the proposed control approach and requires a tight coordination of the power flow from the various energy sources to fix the energy exchange between the microgrid and the utility at the given contractual levels. This necessarily requires a central management of some energy sources (e.g., the utility interfaces), together with the capacity, allowed by three-phase grid-tied inverters, to provide active and reactive power balance among the supply phases. In this way, the power can be exchanged with the utility at unity power factor, as happens in Figure 7 at all times.
- (c) *Fault identification and clearing.* The ability to control the power flow in each specific line of the microgrid requires a coordination of the voltages and currents fed by the grid-tied inverters and is another relevant feature of the proposed control approach. Within reasonable limits, this allows to clear the current in a faulty line by controlling the surrounding energy sources. The faulty line can then be isolated by operating disconnectors at no-load, thus allowing safe servicing. In Figure 7, this capability turns out to be useful during the islanding phase (i.e., 5–7 a.m.) for the lines connecting the microgrid to the utility but can be extended to isolate any other line of the grid.
- (d) *Isolation of sub-grids for maintenance.* This feature extends the previous one to a sequential isolation of more lines, to progressively disconnect an entire sub-grid.
- (e) *Black start.* This feature lies on the presence of utility interfaces at the secondary side of the step-down transformers interfacing the microgrid with the mains. As mentioned before, the UIs perform as voltage sources that are synchronized with the mains during on-grid operation, while they operate as independent voltage sources in off-grid conditions. During the black start, the E-LAN is firstly started up at no load by activating the UIs as voltage sources. The loads are then progressively activated, their power being fed by the ESS. Finally, after a synchronization with the mains voltage, the microgrid reconnects with a controlled ramp-up of the currents at PCC. This behavior is shown in Figure 7 at the end of the islanding phase (i.e., 5–6 a.m.).

7.6. Granularity and Robustness of Control

The proposed simulation spans over 24 h, to show various operating modes that may happen along a typical day. In theory, the granularity of control can reduce to a single period of the line voltage, since the analysis based on phasor representation requires integration of electrical quantities over a line period. In general, the sampling frequency of control must be adapted to the dynamics of controlled quantities (see, e.g., [15]). During transients (e.g., transition from off-grid to on-grid operation), the control quantities should be updated frequently, to prevent overstresses, while during regular operation, the control cycle can slow down to adapt to load variations. From this perspective, the presence of local energy storage smoothing the power steps allows running the central control at a slower timescale, resulting in less electrical stresses and improved robustness of control. Typically, various communication solutions are available with adequate performance when timescales of seconds are considered [21,22].

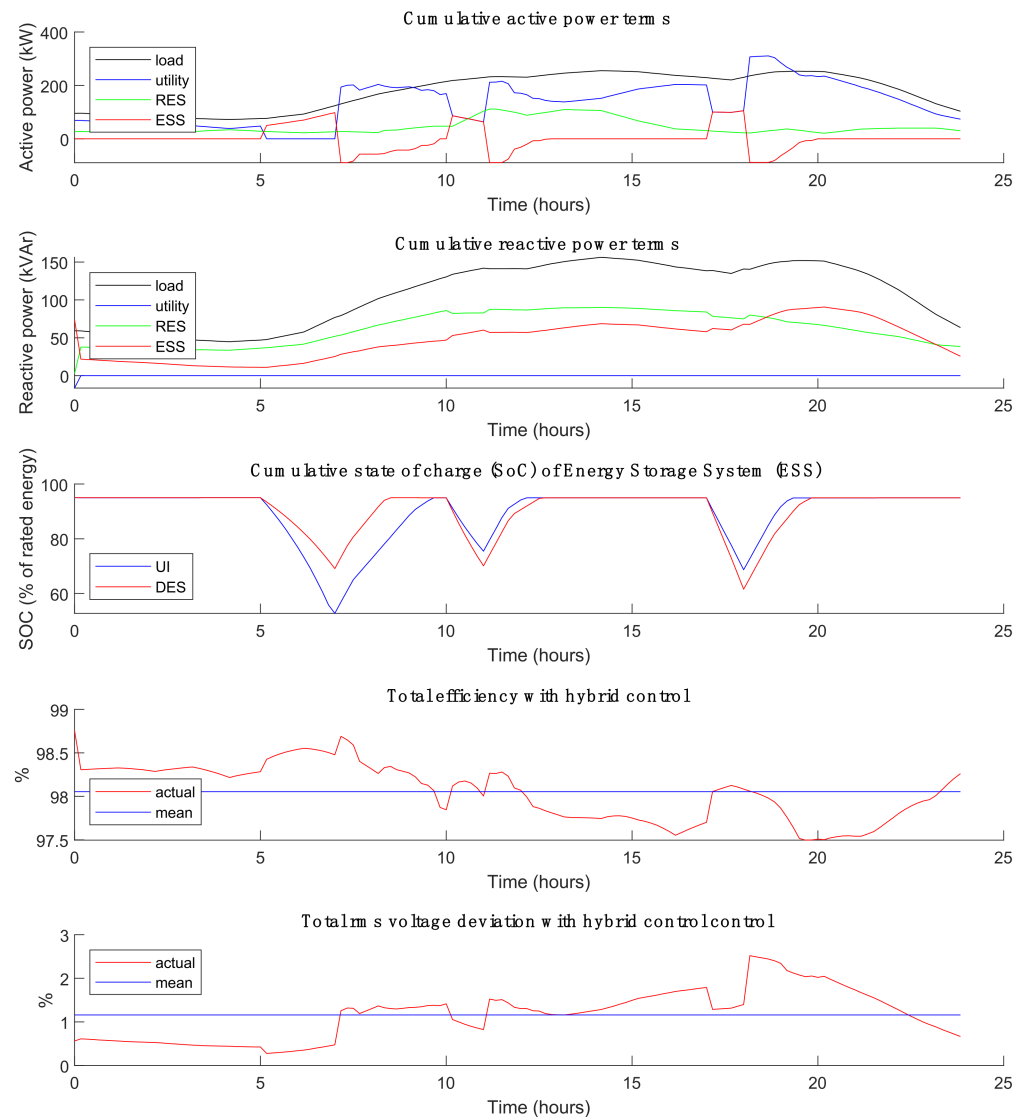


Figure 7. Results obtained with hybrid control.

7.7. Scalability of the Approach

The sample network of Figure 5 includes 55 nodes and 59 branches, representing the typical complexity of LV microgrids fed by MV/LV transformers. In actuality, the proposed control methodology can manage much more complex networks, since the computation algorithm is devised to minimize the number of matrix inversions in each computation step. In particular, only two matrix inversions are required, the size of the matrices being determined by the number of control variables, irrespective of the microgrid complexity.

The approach is scalable not only to handle larger microgrids but also to extend the analysis to the MV domain, where each E-LAN can be considered a single controllable end-user plugged into the MV distribution grid. In this sense, we can extend our analysis from the domain of LV E-LANs to that of MV E-WANs (wide area energy networks) that would set a completely new area of application for microgrid integration and coordination. Even in this case, the involved computation complexity remains practicable, allowing the extension of the optimum control approach to larger high-power networks.

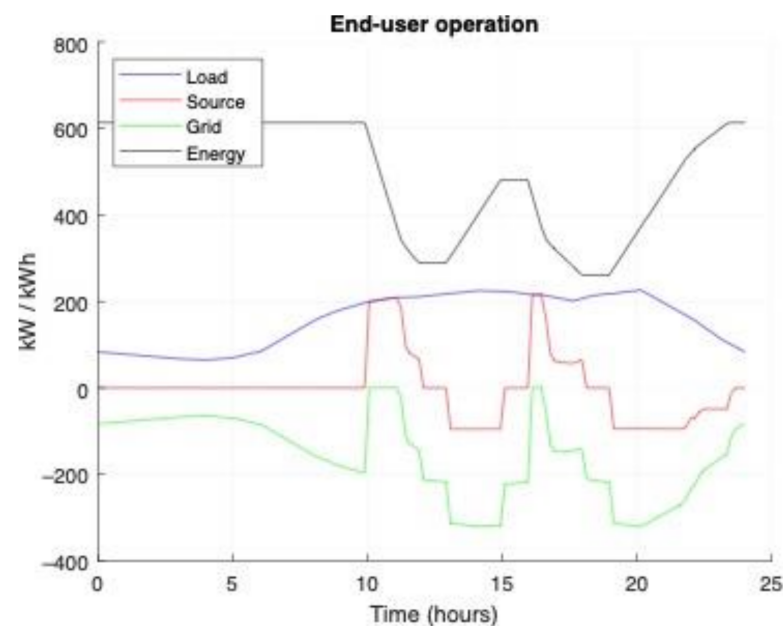


Figure 8. End-users' power and energy behavior in the scenario of Section 7.5a. End-users are equipped with energy storage units rated to feed the local load power for about two hours. Cost of energy is assumed to increase by 50% in the interval 10–12 a.m. and 3–4 p.m., and to halve during night.

8. Conclusions

Under the pressure of recent and incoming directives, the electric market is evolving toward an increasing use of renewable energy sources. A considerable part of these sources will be owned by end-users, who will substantially support the cost for greener electric power systems while aiming at enhancing their role in the energy market. This was already envisioned by the European Union, that plans for 2030 an independent and cost-driven participation of end-users to the electrical market. This sets a great challenge for the reorganization of the energy market, as well as for electric power systems that shall implement substantial technological and structural innovations.

The basic aggregations of the future electric systems will be the microgrids that embrace communities of neighboring end-users and potentially allow, on one side, significant improvement of the electrical performance and, on the other side, direct and independent (or aggregated) participation of end-users to the electric market. To make this possible, however, novel approaches to microgrid design and control shall be adopted.

In this paper, a comprehensive approach to analyze and control meshed microgrids is presented, which aims primarily at the power steering, i.e., the control of active and reactive power in every section of the microgrid. This allows, first, a significant improvement of microgrid performances by taking advantage of the controllability of distributed power sources. Second, power steering means that every user can decide, at any moment, which part of his energy resources can be shared within the microgrid and which is kept for local needs or for trading energy in the market [23].

The developed approach is applicable to AC and DC microgrids of any structure and complexity, irrespective of the nature and variety of end users tied to the microgrid. It sets a solid theoretical basis for future development of user-oriented electrical systems.

Author Contributions: Conceptualization, P.T. and T.C.; methodology, P.T.; software, P.T.; validation, P.T. and T.C.; formal analysis, P.T.; resources, P.T. and T.C.; data curation, P.T., T.C.; writing—original draft preparation, P.T.; writing—review and editing, P.T. and T.C.; project administration, P.T. and T.C. All authors have read and agreed to the published version of the manuscript.

Funding: This research received no external funding.

Institutional Review Board Statement: Not available.

Informed Consent Statement: Not available.

Data Availability Statement: Data available on request.

Conflicts of Interest: The authors declare no conflict of interest.

Appendix A

Details of the application example considered in Sect. are reported in this appendix. In particular, Table A1 specifies the type of feeders, Table A2 shows the connections among grid nodes, the characteristics of the loads tied to the grid, and the parameters of MV/LV transformers feeding the three sub-networks, and Table A3 specifies the characteristics of distributed energy sources.

Table A1. Parameters of the cables used in the application example in Section 7.

Cable Type	Effective Area (mm ²)	R Phase Wire (Ω/km)	L Phase Wire (mH/km)	R Neutral Wire (Ω/km)	L Neutral Wire (mH/km)	Rated Current (A _{rms})
UG1	240	1.63E−01	4.33E−01	4.90E−01	1.50E+00	430
UG2	150	2.66E−01	4.81E−01	7.33E−01	1.81E+00	325
UG3	120	3.26E−01	5.03E−01	8.60E−01	2.01E+00	290
UG4	25	1.54E+00	6.56E−01	2.33E+00	4.63E+00	120
UG5	35	1.11E+00	6.21E−01	1.93E+00	4.03E+00	145
UG6	70	5.69E−01	5.54E−01	1.29E+00	2.75E+00	215
OH1	50	3.87E−01	9.39E−01	6.89E−01	1.50E+00	172
OH2	35	5.24E−01	9.77E−01	8.38E−01	1.56E+00	145
OH3	16	1.15E+00	1.05E+00	1.84E+00	1.69E+00	93
II	150	2.66E−01	4.81E−01	7.33E−01	1.81E+00	325

Table A2. Details about the connections among grid nodes, the characteristics of the loads tied to the grid, and the parameters of MV/LV transformers feeding the three sub-networks considered in the application example in Section 7.

Residential Subnetwork					Commercial Subnetwork					MV/LV Transformers (Yn)				
Line	Node from	Node to	Length (m)	Cable type	Line	Node from	Node to	Length (m)	Cable type	Name	Node from	Node to	kVA	Vcc
R1	R1	R2	35	UG1	C1	C1	C2	30	OH1	RT	R0	R1	500	5%
R2	R2	R3	35	UG1	C2	C2	C3	30	OH1	CT	C0	C1	300	6%
R3	R3	R4	35	UG1	C3	C3	C4	30	OH1	IT	I0	I1	150	2%
R4	R4	R5	35	UG1	C4	C4	C5	30	OH1	Residential loads				
R5	R5	R6	35	UG1	C5	C5	C6	30	UG6	Node	kW	kVAr	Conn	Random term vs. CIGRE profile
R6	R6	R7	35	UG1	C6	C6	C7	30	OH2	R11	13	8	Yn	±40%
R7	R7	R8	35	UG1	C7	C7	C8	30	OH2	R15	60	38	Yn	±40%
R8	R8	R9	35	UG1	C8	C8	C9	30	OH2	R16	46	30	Yn	±40%
R9	R9	R10	35	UG1	C9	C3	C10	30	OH2	R17	4.25	2.65	3n	±40%
R10	R3	R11	35	UG4	C10	C10	C11	30	OH2	R18	40	25	Yn	±40%
R11	R4	R12	35	UG2	C11	C11	C12	30	OH3	Commercial loads				
R12	R12	R13	35	UG2	C12	C11	C13	30	OH3	C12	17	10.5	Yn	±30%
R13	R13	R14	35	UG2	C13	C10	C14	30	OH3	C13	6.8	4.2	Yn	±30%
R14	R14	R15	30	UG3	C14	C5	C15	30	OH3	C14	21.5	13	Yn	±30%
R15	R6	R16	30	UG6	C15	C15	C16	30	OH3	C17	13.5	8.5	Yn	±30%
R16	R9	R17	30	UG4	C16	C15	C17	30	OH3	C18	6.8	4.2	Yn	±30%
R17	R10	R18	30	UG5	C17	C16	C18	30	OH3	C19	21.5	13	Yn	±30%
Residential subnetwork meshing					C18	C8	C19	30	OH3	C20	17	10.5	Yn	±30%
R18	R1	R5	140	UG1	C19	C9	C20	30	UG4	Industrial loads				
R19	R5	R18	200	UG1	Commercial subnetwork meshing					I2	60	37	Yn	20%
Industrial subnetwork					C20	C1	C5	120	UG1					
I1	I1	I2	200	UG2	C21	C5	C20	150	UG1					

Table A3. Characteristics of the distributed energy resources considered in the application example in Section 7.

Type	Node	Inverter Rating (kVA)	Rated/Max Power (kW)	Rated Energy (kWh)	Random Term vs. CIGRE Profile
PV unit	R16	5	4		±20%
	R18	4	3		±20%
	C14	25	20		±20%
	C19	25	20		±20%
	I2	60	50		±20%
Wind turbine	R5	7	5.5		±30%
	C12	25	20		±20%
	C20	25	20		±20%
Energy storage	R10	35	15/30	30	
	C6	35	15/30	30	
	I3	35	15/30	30	
Utility interface	R1	120	50/100	100	
	C1	120	50/100	100	
	I1	80	35/70	70	

References

- Silva, V.A.; Aoki, A.R.; Lambert-Torres, G. Optimal Day-Ahead Scheduling of Microgrids with Battery Energy Storage System. *Energies* **2020**, *13*, 5188. [\[CrossRef\]](#)
- Agostini, M.; Bertolini, M.; Coppo, M.; Fontini, F. The Participation of Small-Scale Variable Distributed Renewable Energy Sources to the Balancing Services Market. *Energy Econ.* **2021**, *97*, 105208. [\[CrossRef\]](#)
- Union, P.O. of the E. *Clean Energy for All Europeans*; European Union: Brussels, Belgium, 2019; p. 24.
- Plancke, G.; De Vos, K.; Belmans, R.; Delnooz, A. Virtual Power Plants: Definition, Applications and Barriers to the Implementation in the Distribution System. In Proceedings of the 2015 12th International Conference on the European Energy Market (EEM), Lisbon, Portugal, 19–22 May 2015; pp. 1–5.
- Popławski, T.; Dudzik, S.; Szeląg, P.; Baran, J. A Case Study of a Virtual Power Plant (VPP) as a Data Acquisition Tool for PV Energy Forecasting. *Energies* **2021**, *14*, 6200. [\[CrossRef\]](#)
- Subramanya, R.; Yli-Ojanperä, M.; Sierla, S.; Hölttä, T.; Valtakari, J.; Vyatkin, V. A Virtual Power Plant Solution for Aggregating Photovoltaic Systems and Other Distributed Energy Resources for Northern European Primary Frequency Reserves. *Energies* **2021**, *14*, 1242. [\[CrossRef\]](#)
- Abedini, H.; Caldognetto, T.; Mattavelli, P.; Tenti, P. Real-Time Validation of Power Flow Control Method for Enhanced Operation of Microgrids. *Energies* **2020**, *13*, 5959. [\[CrossRef\]](#)
- Simmini, F.; Caldognetto, T.; Bruschetta, M.; Mion, E.; Carli, R. Model Predictive Control for Efficient Management of Energy Resources in Smart Buildings. *Energies* **2021**, *14*, 5592. [\[CrossRef\]](#)
- Mazumder, S.K.; Kulkarni, A.; Sahoo, S.; Blaabjerg, F.; Mantooth, H.A.; Balda, J.C.; Zhao, Y.; Ramos-Ruiz, J.A.; Enjeti, P.N.; Kumar, P.R.; et al. A Review of Current Research Trends in Power-Electronic Innovations in Cyber-Physical Systems. *IEEE J. Emerg. Sel. Topics Power Electron.* **2021**, *9*, 5146–5163. [\[CrossRef\]](#)
- Matevosyan, J.; MacDowell, J.; Miller, N.; Badrzadeh, B.; Ramasubramanian, D.; Isaacs, A.; Quint, R.; Quitmann, E.; Pfeiffer, R.; Urdal, H.; et al. A Future With Inverter-Based Resources: Finding Strength From Traditional Weakness. *IEEE Power Energy Mag.* **2021**, *19*, 18–28. [\[CrossRef\]](#)
- Buticchi, G.; Lam, C.-S.; Ruan, X.; Liserre, M.; Barater, D.; Benbouzid, M.; Gomis-Bellmunt, O.; Paja, C.; Kumar, C.; Zhu, R. The Role of Renewable Energy System in Reshaping the Electrical Grid Scenario. *IEEE Open J. Ind. Electron. Soc.* **2021**, *2*, 451–468. [\[CrossRef\]](#)
- Zafeiratou, I.; Prodan, I.; Lefèvre, L. A Hierarchical Control Approach for Power Loss Minimization and Optimal Power Flow within a Meshed DC Microgrid. *Energies* **2021**, *14*, 4846. [\[CrossRef\]](#)
- Simmini, F.; Agostini, M.; Coppo, M.; Caldognetto, T.; Cervi, A.; Lain, F.; Carli, R.; Turri, R.; Tenti, P. Leveraging Demand Flexibility by Exploiting Prosumer Response to Price Signals in Microgrids. *Energies* **2020**, *13*, 3078. [\[CrossRef\]](#)
- Balabanian, N.; Bickart, T.A. *Electrical Network Theory*; Wiley: New York, NY, USA, 1969; ISBN 978-0-471-04576-2.
- Ela, E.; O'Malley, M. Studying the Variability and Uncertainty Impacts of Variable Generation at Multiple Timescales. *IEEE Trans. Power Syst.* **2012**, *27*, 1324–1333. [\[CrossRef\]](#)

16. CIGRE Task Force C6. 04.02. In *Benchmark Systems for Network Integration of Renewable and Distributed Energy Resources*; International Council on Large Electric Systems: Paris, France, 2014.
17. Caldognetto, T.; Tenti, P. Microgrids Operation Based on Master–Slave Cooperative Control. *IEEE J. Emerg. Sel. Top. Power Electron.* **2014**, *2*, 1081–1088. [[CrossRef](#)]
18. Rosso, R.; Wang, X.; Liserre, M.; Lu, X.; Engelken, S. Grid-Forming Converters: Control Approaches, Grid-Synchronization, and Future Trends—A Review. *IEEE Open J. Ind. Applicat.* **2021**, *2*, 93–109. [[CrossRef](#)]
19. Caldognetto, T.; Abedini, H.; Mattavelli, P. A Per-Phase Power Controller for Smooth Transitions to Islanded Operation. *IEEE Open J. Power Electron.* **2021**, *2*, 636–646. [[CrossRef](#)]
20. Wang, J.; Zhou, N.; Ran, Y.; Wang, Q. Optimal Operation of Active Distribution Network Involving the Unbalance and Harmonic Compensation of Converter. *IEEE Trans. Smart Grid* **2019**, *10*, 5360–5373. [[CrossRef](#)]
21. Burgos, R.; Sun, J. The Future of Control and Communication: Power Electronics-Enabled Power Grids. *IEEE Power Electron. Mag.* **2020**, *7*, 34–36. [[CrossRef](#)]
22. Dambrauskas, P.; Syed, M.H.; Blair, S.M.; Irvine, J.M.; Abdulhadi, I.F.; Burt, G.M.; Bondy, D.E.M. Impact of Realistic Communications for Fast-Acting Demand Side Management. *CIREN-Open Access Proc. J.* **2017**, *2017*, 1813–1817. [[CrossRef](#)]
23. Shezan, S.A.; Hasan, K.N.; Rahman, A.; Datta, M.; Datta, U. Selection of Appropriate Dispatch Strategies for Effective Planning and Operation of a Microgrid. *Energies* **2021**, *14*, 7217. [[CrossRef](#)]